

## Article

# Transient Modulation for the Step-Load-Change Process in a Dual-Bridge Series Resonant Converter †

Hui Xu <sup>1,2</sup> , Shengzhi Zhou <sup>2</sup>, Xiaodong Li <sup>2</sup> , Hao Chen <sup>3</sup> and Song Hu <sup>1,\*</sup> 

<sup>1</sup> School of Electrical Engineering and Automation, Changshu Institute of Technology, Suzhou 215000, China; must\_hxu@outlook.com

<sup>2</sup> Faculty of Information Technology, Macau University of Science and Technology, Macau 999078, China; must\_zsz@hotmail.com (S.Z.); xqli@must.edu.mo (X.L.)

<sup>3</sup> School of Electrical and Power Engineering, China University of Mining and Technology, Xuzhou 221116, China; hchen@cumt.edu.cn

\* Correspondence: husong@csitg.edu.cn

† This paper is an extended version of our paper published in Fast Transient Modulation of a Dual-Bridge Series Resonant Converter. In Proceedings of the IECON 2021—47th Annual Conference of the IEEE Industrial Electronics Society Conference, Toronto, ON, Canada, 13–16 October 2021.

**Abstract:** A phase-shifted dual-bridge series resonant DC-DC converter (DBSRC) is a competitive candidate for applications of an energy storage system. At the request of a step-load-change command such as the start-up and power-level change, the converter may suffer from large-amplitude transient oscillations due to improper transient modulation. Furthermore, the DC bias current and overshoot current/voltage in the resonant tank and transformer caused by oscillations may result in transformer saturation and poor dynamic performance. To solve these problems, two fast transient modulation (FTM) methods are proposed in this paper. First, based on the steady-state analysis of the converter with phase-shift control, the current and voltage trajectory of the resonant capacitor can be obtained. Then, the detailed principles of two FTM methods are explained for achieving a smooth transition. Through the adjustment of the durations of the adjacent switching intervals temporarily, the transient trajectory can be predicted and is expected to match the destination trajectory within one switching period. Consequently, the proposed FTM methods enable the converter to move from one steady state to another instantly and the step-load-change transition can be an overshoot-free procedure. Finally, both simulation and experimental tests prove that the two modulation methods can effectively eliminate DC bias current and overshoot current/voltage in the DBSRC transient process and obtain a fast transient response.

**Keywords:** DC bias; transient performance; transient modulation



**Citation:** Xu, H.; Zhou, S.; Li, X.; Chen, H.; Hu, S. Transient Modulation for the Step-Load-Change Process in a Dual-Bridge Series Resonant Converter. *Electronics* **2022**, *11*, 822. <https://doi.org/10.3390/electronics11050822>

Academic Editor: Carlos Andrés García-Vázquez

Received: 30 January 2022

Accepted: 3 March 2022

Published: 6 March 2022

**Publisher's Note:** MDPI stays neutral with regard to jurisdictional claims in published maps and institutional affiliations.



**Copyright:** © 2022 by the authors. Licensee MDPI, Basel, Switzerland. This article is an open access article distributed under the terms and conditions of the Creative Commons Attribution (CC BY) license (<https://creativecommons.org/licenses/by/4.0/>).

## 1. Introduction

With the fast development of distributed power generation and energy storage facilities, efficient power conversion technologies have become hotspots in the research field of power electronics [1,2]. Among various kinds of power electronics systems, the isolated bidirectional DC-DC converter (IBDC) has gained considerable attention since it can manipulate the power flow magnitude and direction between two DC buses with different voltage levels [3]. The dual-active-bridge (DAB) type of isolated converter is one typical topology of IBDC that is featured with high power density and control simplicity [4,5]. Connected to an LC resonant tank, the dual-bridge series resonant DC-DC converter (DBSRC) is evaluated experimentally in [6]. The main operation characteristics of DBSRC with the fundamental harmonic approximation (FHA) method are discussed in [7]. However, FHA method is unable to predict a state accurately since the FHA only considers the fundamental component. In [8], an accurate DBSRC model is established according to the characteristics of power transfer and switching behavior. Most reported literature are concerned with

steady-state analysis with different optimal modulation controls for minimized loss [9,10]. Various hybrid control methods in which switching frequency modulation is combined with phase-shift modulation are proposed to extend soft-switching regions [11,12]. The reactive power is set as the optimized objective and solved using particle swarm optimization method in [13]. Later, in [14,15], to depress the conduction loss, a minimum current modulation scheme with asymmetric-adjusted PWM is investigated.

Although the steady-state performance of a DBSRC has been significantly improved, those optimized modulations cannot enhance transient-state performance of DBSRC. The single-loop control strategy is the mainstream feedback control strategy for DBSRC, where the dynamic model is determined by measurement voltage error only. Due to the digital delay in transport process, the fast dynamic response cannot be implemented directly in DBSRC with single-loop control. Hence, on the simplified average model, a dynamic model with average input and output voltage is proposed to improve the dynamic response [16]. A small-signal model of DBSRC is further introduced in [17] and model-predictive control has been investigated in [18]. All these feedback control strategies ignore the transient state in the analysis as the converter adapts to different transfer power demands. The transient process from one load to another, even though the series capacitor can block the DC component in steady state, may have transient voltage/current oscillations due to improper transient modulation. Meanwhile, the oscillations in the resonant tank might induce the saturation of the high-frequency transformer, causing slow and uneven transient response [19,20]. To eliminate the DC bias current, a fast transient phase-shift strategy is initially proposed for a DAB converter [21]. By adopting the fast transient phase-shift strategy, all possible transient processes are discussed in detail [22]. Some improved transient phase-shift strategies have been developed to reduce the DC bias current [23,24]. In [25], the DC bias current can be eliminated at the expense of ZVS operation. A state machine is designed for different working mode transitions in [26]. A universal solution for all the transient states with seamless transient processes is investigated in [27]. However, these phase-shift strategies are optimized for non-resonant transient-state converters and need to select the switching pattern for multiple working modes, which complicates the implementation of the control strategy. There has been little quantitative analysis of dynamic phase-shift strategy for resonant transient-state converters. A trajectory-switching modulation strategy is proposed to suppress high-frequency transient oscillations for DBSRC [28]. Using state-plane analysis, an optimal trajectory for an LLC transient-state converter is proved [29]. A dynamic control strategy of a DBSRC converter based on trajectory prediction is proposed in [30]. However, in [29,30], the cost of trajectory estimation is the increasing complexity level of control.

In general, with a conventional low-gain PI controller, no matter what modulation method is used, it executes only a small change of phase-shift angle in every switching cycle to produce a smooth but slow dynamic response. Although the converter can have an oscillation-free performance, the total transient process is long. A high-gain controller leads to a smaller steady-state tracking error, but also gives rise to a more abrupt and larger transient variation of phase-shift angle, which tends to produce undesirable large-amplitude high-frequency transient oscillations if no special measurement is used. This paper proposes two fast transient modulation (FTM) methods to achieve a fast and overshoot-free step-load change process. The two methods will adjust the durations of switching intervals to match the predicted ones. Thus, it can effectively solve large overshoot current and long transient response time in the transient process and obtain a fast transient response. The work was presented in [31] and has been extensively expanded with more investigation detail and experimental results. The outline of this paper is as follows. Section 2 presents the operating principle of the converter with phase-shift control, and the steady-state trajectory can be obtained. Two fast transient modulation methods at the step-load-change transition are then developed in Section 3. In Section 4, both simulation and experimental tests are conducted to verify the effectiveness of the proposed modulation methods. Finally, conclusions are drawn in Section 5.

### 2. Steady-State Operation of a DBSRC

The topology of a DBSRC is presented in Figure 1. Two DC voltage sources are connected with their active H bridges respectively, which are connected by a series resonant tank and a high-frequency(HF) isolation transformer. The resonant tank voltage and current are  $v_{LC}$  and  $i_s$ . The resonant capacitor voltage is  $v_C$ . The turns ratio of the HF transformer is  $n_t : 1$ . It is assumed in this work that the conduction angle of each switch is  $180^\circ$  and two switches in each bridge arm are operated complementarily. As a result, the two HF AC voltages  $v_{AB}$  and  $v_{CD}$  are square-wave with a duty ratio of 0.5, whose amplitudes are  $V_p$  and  $V_s$ , respectively.

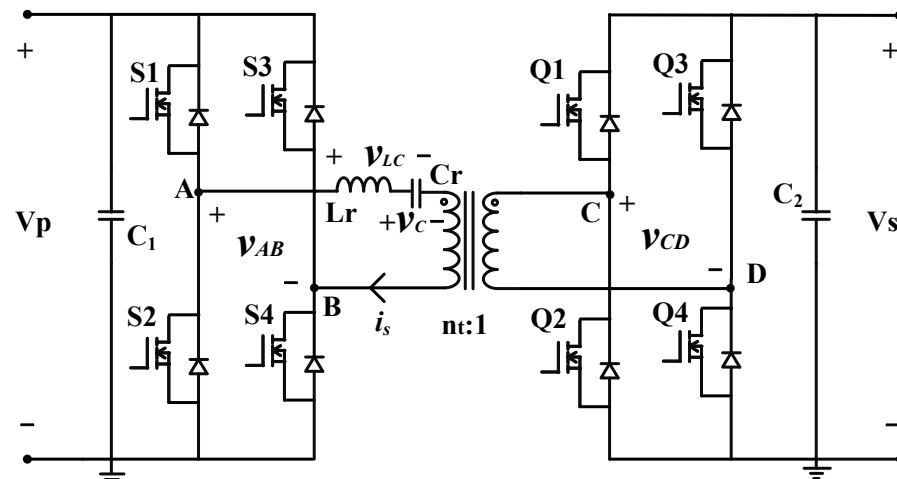


Figure 1. Topology of a dual-bridge series resonant DC-DC converter.

The steady-state waveform of DBSRC is illustrated in Figure 2.  $DT$  is the phase-shift between  $v_{AB}$  and  $v_{CD}$ , where  $D \in [-0.5, 0.5]$  is the phase-shift ratio. The HF switching period is  $2T$ . One HF switching period can be divided into four modes, in each of which the resonant tank voltage  $v_{LC}$  is different. Referring to Figure 2, values of  $v_{LC}$  in each mode are  $V_p + V'_s$ ,  $V_p - V'_s$ ,  $-(V_p + V'_s)$ ,  $-(V_p - V'_s)$  respectively.  $V'_s = n_t V_s$  is the primary side referred secondary DC source voltage.

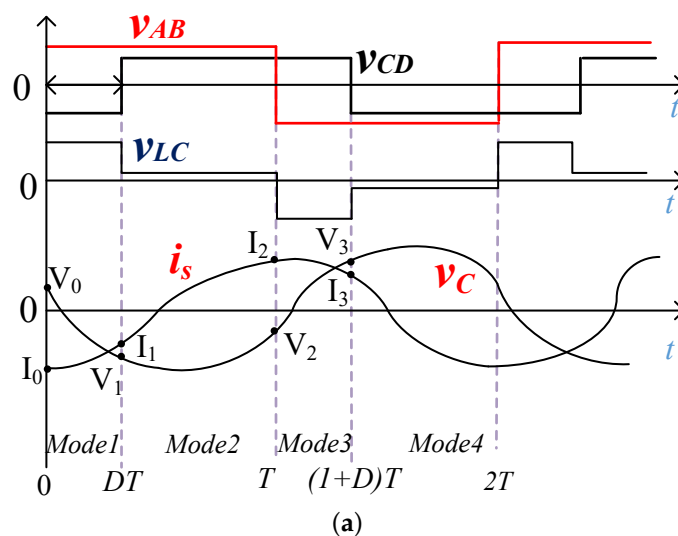


Figure 2. Cont.

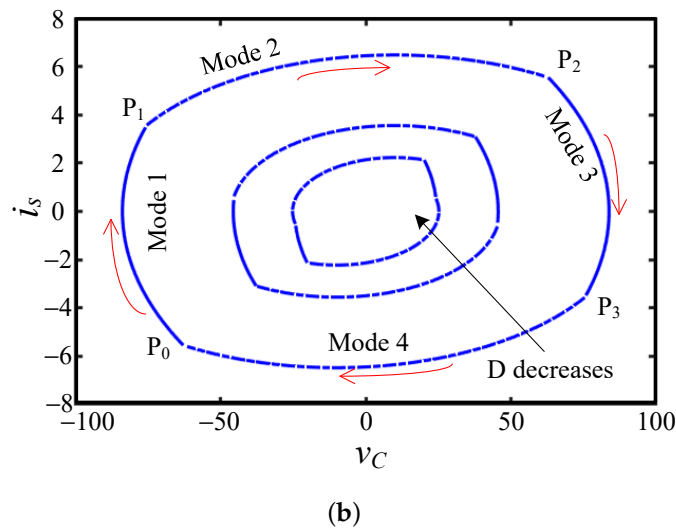


Figure 2. (a) Steady -state waveforms of DBSRC; (b) Steady-state trajectory of  $i_s$ - $v_C$  for different  $D$ .

Applying Kirchhoff’s Voltage Law (KVL) and characteristics of LC, the following differential equations using  $v_C$  and current  $i_s$  as variables are obtained:

$$\begin{cases} v_{LC} = v_C + L_r \frac{di_s}{dt} \\ i_s = C_r \frac{dv_C}{dt} \end{cases} \tag{1}$$

The general solutions can be obtained and given as:

$$\begin{cases} i_s = I_i \cos \alpha + \frac{v_{LC} - V_i}{Z_r} \sin \alpha \\ v_C = I_i Z_r \sin \alpha + v_{LC} + (V_i - v_{LC}) \cos \alpha \end{cases} \tag{2}$$

where  $I_i$ ,  $V_i$  are the initial values of  $i_s$  and  $v_C$  in the mode, respectively. The switching frequency is  $f_s = 1/(2T)$ , the resonant frequency is  $f_r = \frac{1}{2\pi(\sqrt{L_r C_r})}$ , and  $Z_r = \sqrt{L_r/C_r}$  is the characteristic impedance of the resonant circuit. The normalized switching frequency is  $F = f_s/f_r$  and  $\alpha = \omega_s t/F$ .

Since both  $i_s$  and  $v_C$  are periodic signals, the values of them at the boundary points between each mode can be found by solving the differential equations of each mode in sequence. With the help of Equation (2), the values of current  $i_s$  and voltage  $v_C$  at  $t = 0$  and  $t = DT$  are obtained:

$$\begin{cases} I_0(D) = -\frac{V_p}{Z_r} [M \sin(\frac{D\pi}{F}) + [1 - M \cos(\frac{D\pi}{F})] \tan(\frac{\pi}{2F})] \\ I_1(D) = \frac{V_p}{Z_r} [\sin(\frac{D\pi}{F}) + [M - \cos(\frac{D\pi}{F})] \tan(\frac{\pi}{2F})] \\ V_0(D) = -2V_p M \sec(\frac{\pi}{2F}) \sin(\frac{(1-D)\pi}{2F}) \sin(\frac{D\pi}{2F}) \\ V_1(D) = -2V_p \sec(\frac{\pi}{2F}) \sin(\frac{(1-D)\pi}{2F}) \sin(\frac{D\pi}{2F}) \end{cases} \tag{3}$$

where  $M = V'_s/V_p = n_t V_s/V_p$  is the voltage gain. It should be noted that those values are functions of the phase-shift ratio  $D$ . Due to the anti-symmetry features in steady-state operation, the values at  $t = T$  and  $t = (1 + D)T$  can be obtained easily with help of Equation (3).

According to the analysis results, the steady-state trajectory of  $i_s$  and  $v_C$  can be drawn as a closed loop for a given phase-shift ratio  $D$ , which is illustrated in Figure 2b. A larger

phase-shift ratio  $D$  will result in a loop with larger size. The moving direction in the loop is clockwise and the sequence of mode is  $1 \rightarrow 2 \rightarrow 3 \rightarrow 4$  for a positive  $D$ . The coordinates of boundary point  $P_n$  is  $(V_n, I_n)$  with  $n = 0, 1, 2, 3$ , which are the boundary values marked in Figure 2a.

### 3. Transient Modulation at the Step-Load-Change Transition

With the phase-shift control, the transmission power of a DBSRC is proportional to  $\sin(D\pi)$  [6]:

$$P_o = \frac{8n_t V_p V_s}{\pi^2 (\omega_s L_r - \frac{1}{\omega_s C_r})} \sin(D\pi) \tag{4}$$

At the request of a step-load-change command,  $D$  is supposed to have a corresponded step change too. It is assumed that the converter has an initial phase-shift is  $DT$ , and the final phase-shift is  $(D + d)T$ . Apparently, the adjustment  $dT$  can be completed by modulating the gating signals of the eight switches in many different ways.

#### 3.1. DTM

The simplest and direct way, named direct transient modulation (DTM), can be described as follows: the gating signals of one of the two bridges are fixed, while the gating signals of the other bridge are shifted directly as required. As an example, the process of DTM with  $d > 0$  is illustrated in Figure 3. The primary HF AC voltage  $v_{AB}$  is assumed to be fixed, and the position of  $v_{CD}$  is moved by  $dT$  through the modulation of gating signals of  $Q_1 \sim Q_4$ . For the waveform of  $v_{CD}$  in the figure, the dotted line represents the original waveform and the solid one represents the modified waveform. During the transition procedure, the duration of Mode 1 is lengthened by  $dT$  by delaying the rising edge of  $v_{CD}$ . The durations of followed pulses of  $v_{CD}$  remain at  $T$ . Consequently, in the followed regular period, the phase-shift between the two square voltages becomes  $(D + d)T$ .

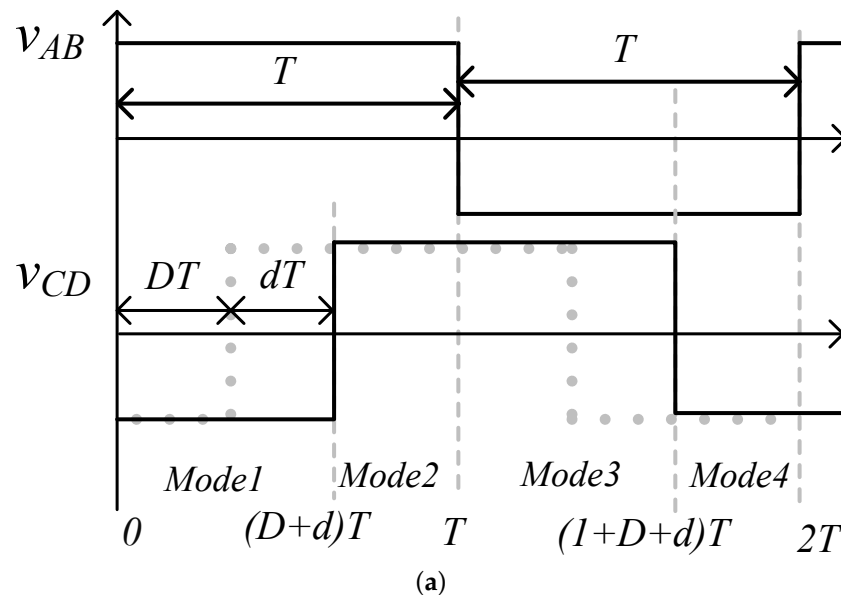
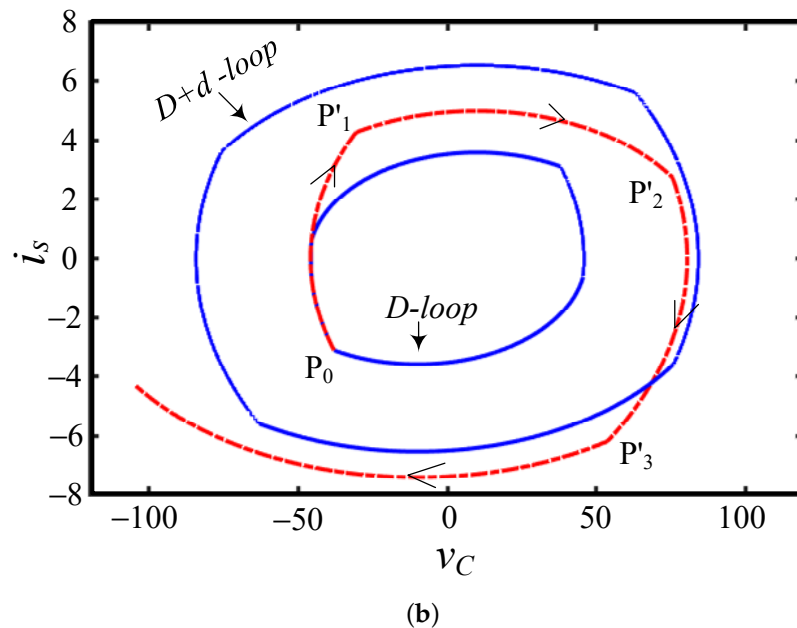


Figure 3. Cont.



**Figure 3.** The principle of DTM: (a) the transient waveforms of  $v_{AB}$  and  $v_{CD}$ ; (b) the transient trajectory of  $v_C$  and  $i_s$ .

In another view angle, the step-load change process using DTM can be observed from the trajectory of  $v_C$  and  $i_s$  shown in Figure 3b. It can be seen that the process starts from  $P_0$  on the small loop of  $D$  and moves to  $P'_1, P'_2, P'_3$  in sequence. However, the followed trajectory cannot match the loop of  $(D + d)$  instantly. Apparently, the transient process would have some oscillations and the track outside of the large  $(D + d)$ -loop means overshoot voltage and overshoot current. In theory, this process would last and cause unrespectable damage. In practical conditions, the oscillation would gradually diminish, and the trajectory would finally settle down to the loop of  $D + d$  thanks to the damping effect of parasitic resistance in the circuit. However, the parasitic resistance may cause extra conduction loss and should be minimized during actual circuit design and implementation.

### 3.2. Proposed FTM

To improve the step-change transient response, a fast transient modulation (FTM) is proposed in the current work. The objective is to let the original trajectory move naturally from the original loop to the final loop within one cycle. During the transient process, the durations of each mode should be adjusted properly so that the final values of  $v_C$  and  $i_s$  at the end of transient process should perfectly match the values at the beginning of a new period with the final phase-shift ratio.

Based on the observation of those trajectories, it can be concluded that the curvature of each mode is fixed and decided by the value of  $v_{LC}$ . The absolute values of  $v_{LC}$  in Mode 1 and 3 is the sum of two terminal voltages, which is larger than that in Mode 2 and 4. Consequently, the trajectories (or waveforms of  $v_C$  and  $i_s$ ) in Mode 1 and 3 have high dynamics, which should be used to speed up the transient process.

Unlike in DTM, the HF AC voltages on both sides are to be shifted in FTM. Two modulation factors  $x$  and  $y$  are introduced to define the change of the rising or falling edge of  $v_{AB}$  and  $v_{CD}$ , which in turn indicate the change of switching moment of  $S_1$ – $S_4$  and  $Q_1$ – $Q_4$ . The positive direction of  $x$  is defined to the right, while the positive direction of  $y$  is to the left. According to the number of steps involved, two methods based on FTM are to be discussed.

### 3.2.1. FTM-I with Three Steps

The first proposed method has three steps in the transient process. The basic idea of FTM-1 is exemplified with  $d > 0$  (a step-up of  $D$ ) in Figure 4a with the trajectory of  $i_s$  and  $v_C$ . It is seen that the whole process consists of three steps:  $P_0$ - $P'_1$ - $P'_2$ - $P'_3$ . As mentioned, initially Mode 1 ( $P_0$ - $P'_1$ ) is used to move from the initial  $D$ -loop to the outside  $(D + d)$ -loop, which is extended by  $xT$  until it stops at  $P'_1$ . With another unknown phase-shift  $yT$ , Mode 2 continues, and it is expected to reach Mode 3 of the final loop. The proper selection of  $x$  and  $y$  should let the third step  $P'_2$ - $P'_3$  be the part of  $(D + d)$ -loop. Starting from  $P'_3$ , a new steady state begins. In addition, the whole process is located between the two loops, which indicates no overshoot voltage or current existing.

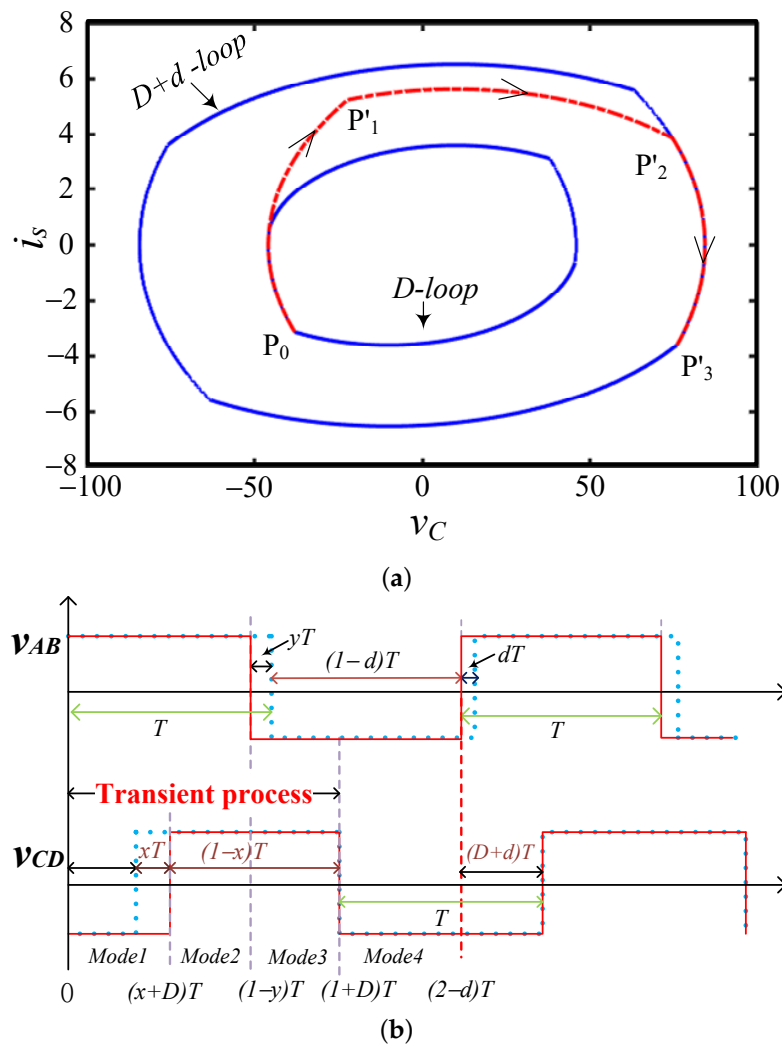


**Figure 4.** Principle of FTM-I with three steps for  $d > 0$ : (a) the transient trajectory of  $i_s$  and  $v_C$ ; (b) the transient waveforms of  $v_{AB}$  and  $v_{CD}$ .

The modifications on the waveforms of  $v_{AB}$  and  $v_{CD}$  in the transient process are shown in Figure 4b. During the transient, the resonant current and voltage can be evaluated as follows.

Mode 1 ( $t \in [0, (D + x)T]$ ): The rising edge of  $v_{CD}$  is delayed by  $xT$  so that the duration of Mode 1 is extended from  $DT$  to  $(D + x)T$ . At the end of this step,  $v_C$  and  $i_s$  are calculated as:

$$\begin{cases} I'_1 = I_o \cos \beta_1 + \frac{V_p + V'_s - V_o}{Z_r} \sin \beta_1 \\ V'_1 = I_o Z_r \sin \beta_1 + (V_p + V'_s) - [V_p + V'_s - V_o] \cos \beta_1 \end{cases} \quad (5)$$

where  $\beta_1 = \frac{(D+x)\pi}{F}$  and  $I_o, V_o$  are obtained from Equation (3).

Mode 2 ( $t \in [(D + x)T, (1 - y)T]$ ): The falling edge of  $v_{AB}$  is delayed by  $yT$  and the duration of Mode 2 is changed to  $(1 - D - x - y)T$ . At the end of this step,  $v_C$  and  $i_s$  are calculated as:

$$\begin{cases} I'_2 = I'_1 \cos \beta_2 + \frac{V_p - V'_s - V'_1}{Z_r} \sin \beta_2 \\ V'_2 = I'_1 Z_r \sin \beta_2 + (V_p - V'_s) - [V_p - V'_s - V'_1] \cos \beta_2 \end{cases} \quad (6)$$

where  $\beta_2 = \frac{(1-y-D-x)\pi}{F}$ .

Mode 3 ( $t \in [(1 - y)T, (1 + D)T]$ ): the falling edge of  $v_{CD}$  is not changed so that the duration of Mode 3 is  $(D + y)T$ . At the end of this step,  $v_C$  and  $i_s$  are calculated as:

$$\begin{cases} I'_3 = I'_2 \cos \beta_3 - \frac{V_p + V'_s + V'_2}{Z_r} \sin \beta_3 \\ V'_3 = I'_2 Z_r \sin \beta_3 - (V_p + V'_s) + [V_p + V'_s + V'_2] \cos \beta_3 \end{cases} \quad (7)$$

where  $\beta_3 = \frac{(D+y)\pi}{F}$ .

Mode 4 ( $t \in [(1 + D)T, (2 - d)T]$ ): the next rising edge of  $v_{AB}$  is shifted earlier by  $dT$  and consequently the duration of Mode 4 is  $(1 - D - d)T$  which matches the new steady state. As a result,  $I'_3$  and  $V'_3$  can be regarded as the initial values of current and voltage of the new steady state. According to Equation (3),  $I'_3$  and  $V'_3$  can be expressed as:

$$\begin{cases} I'_3 = \frac{V_p}{Z_r} \left[ \sin \frac{(D+d)\pi}{F} + (M - \cos \frac{(D+d)\pi}{F}) \tan \frac{\pi}{2F} \right] \\ V'_3 = -2V_p \sec \frac{\pi}{2F} \sin \frac{(1-D-d)\pi}{2F} \sin \frac{(D+d)\pi}{2F} \end{cases} \quad (8)$$

Equaling (7) to (8), the values of  $x$  and  $y$  can be solved.

In the case of  $d < 0$ , a similar process can be performed, and the principle is illustrated in Figure 5. It is seen that the whole process starts from Mode 2 ( $P_1 - P'_2$ ) with a reduced duration  $(1 - d - y)T$  and Mode 3 is used to approach the small loop of  $(D + d)$  at  $P'_3$ . Part of Mode 4 perfectly coincides with that of the final state loop and the new state-state begins at  $P'_4$ .

In conclusion, FTM-I consists of three different modes. Variables  $x$  and  $y$  are associated with the modulation of  $v_{CD}$  and  $v_{AB}$  respectively. During the transient process, only one edge of  $v_{CD}$  is shifted to the right or delayed by  $xT$ , where  $x$  has the same polarity as that of  $d$ . For the waveform of  $v_{AB}$ , the falling edge is shifted to the left by  $yT$ , where  $y$  is positive regardless of the polarity of  $d$ . The next falling edge with all followed edges is shifted earlier by  $dT$ . Consequently,  $v_{CD}$  has two transient pulses, whose width is  $(1 + x)T$  and  $(1 - x)T$  respectively.  $v_{AB}$  only has one transient pulse with the width at  $(1 + y - d)T$ . The durations of each mode in the transient process are concluded in Table 1.

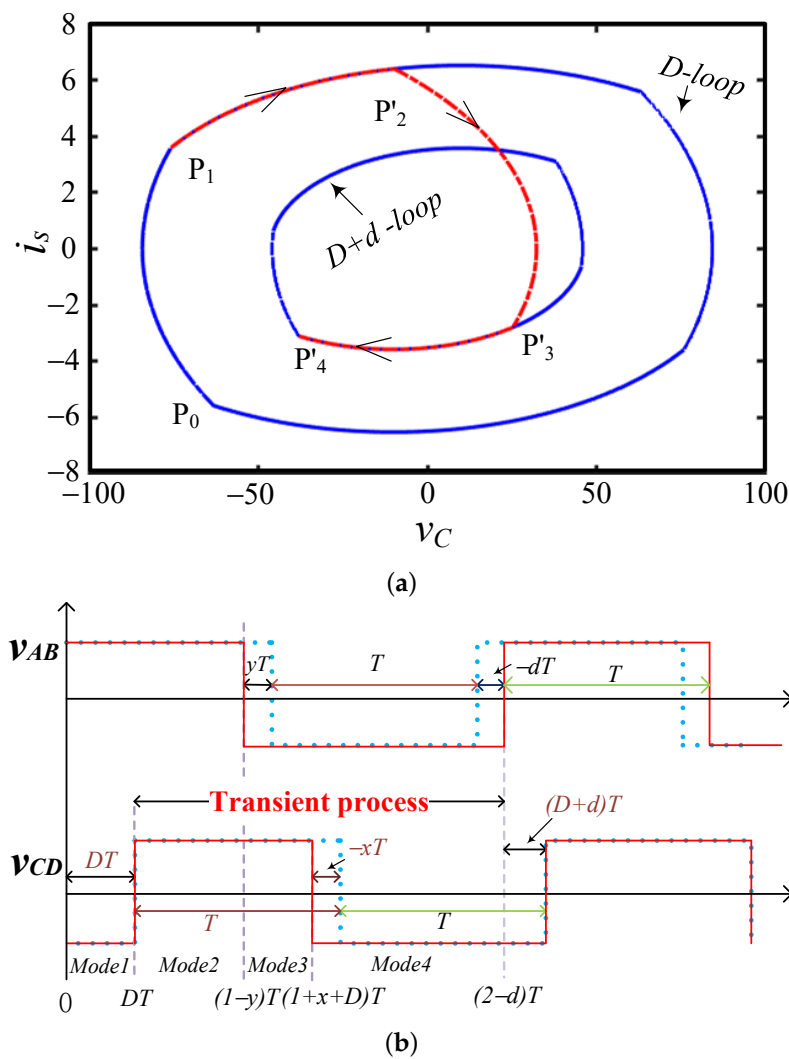


**Figure 5.** Principle of FTM-I with three steps for  $d < 0$ : (a) the transient trajectory of  $i_s$  and  $v_C$ ; (b) the transient waveforms of  $v_{AB}$  and  $v_{CD}$ .

**Table 1.** The durations of each mode using FTM-I.

	$d > 0$	$d < 0$
Mode 1	$(D + x)T$	$DT$
Mode 2	$(1 - D - x - y)T$	$(1 - D - y)T$
Mode 3	$(D + y)T$	$(D + x + y)T$
Mode 4	$(1 - D - d)T$	$(1 - D - x - d)T$

### 3.2.2. FTM-II with Two Steps

The basic idea of FTM-II is also exemplified with  $d > 0$  (a step-up of  $D$ ). According to the trajectory of  $i_s$  and  $v_C$  in Figure 6a, two variables  $x$  and  $y$  are introduced to define the durations of two transient steps. As with FTM-I, the duration of Mode 1 is increased by  $xT$  to let the trajectory cut into the  $(D + d)$ -loop at  $P'_1$  quickly. As part of  $(D + d)$ -loop already, the duration of Mode 2 is adjusted to stop right at the boundary point  $P'_2$  of  $(D + d)$ -loop, which is attributed to the proposed selections of  $x$  and  $y$ . Therefore, the converter enters a new steady state now after a two-step transient process of  $P_0$ - $P'_1$ - $P'_2$ . Again, no overshoot voltage or current exists since the transient trajectory is completely between the two loops. During the transient process, the current and voltage can be evaluated as follows referring to Figure 6b.

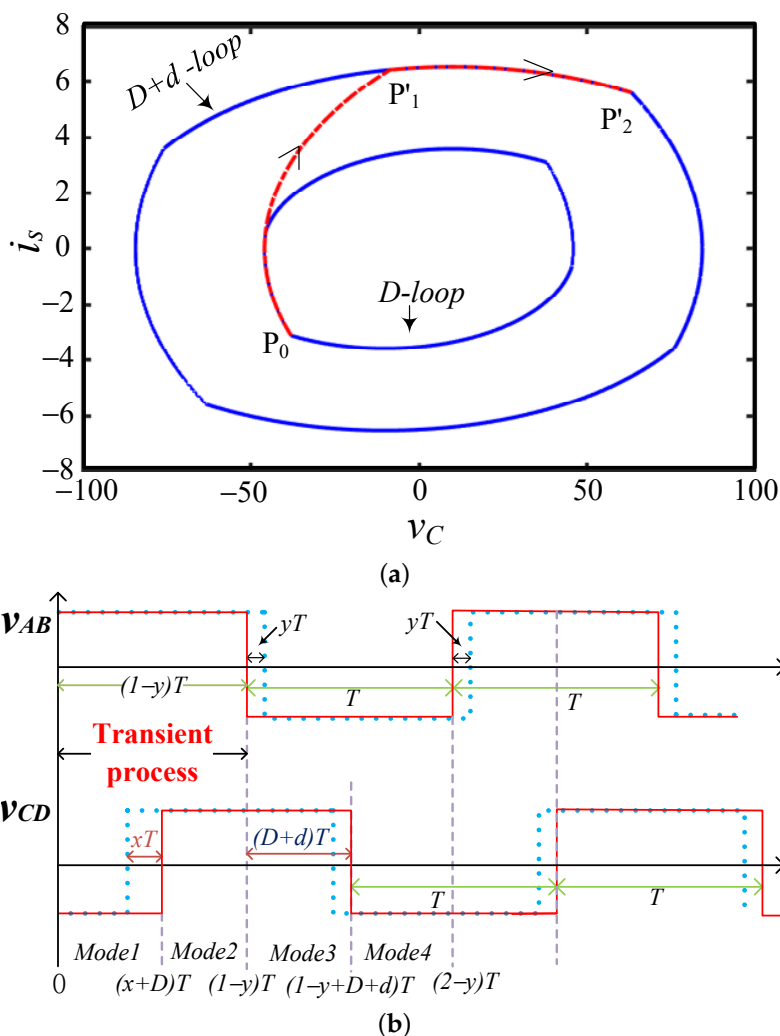


**Figure 6.** Principle of FTM-II with two steps for  $d > 0$ : (a) the transient trajectory of  $i_s$  and  $v_C$ ; (b) the transient waveforms of  $v_{AB}$  and  $v_{CD}$ .

In the first two modes of FTM-II, the calculations for  $i_s$ ,  $v_C$  are exactly the same as Equations (5) and (6), i.e., Mode 1 has a duration of  $(D + x)T$  and Mode 2 has a duration of  $(1 - D - x)T$ . The next falling edge of  $v_{CD}$  is purposely shifted so that the duration of Mode 3 is  $(D + d)T$  and the followed pulses all have regular duration of  $T$ . Therefore, if the values of the voltage and current at the end of Mode 2 are forced to be equal to the corresponding values in the final steady state, and the converter can enter the new steady state instantly. According to Equation (3),  $I'_2$  and  $V'_2$  are expected to be:

$$\begin{cases} I'_2 = -\frac{V_p}{Z_r} [M \sin \frac{(D+d)\pi}{F} + (1 - M \cos \frac{(D+d)\pi}{F}) \tan \frac{\pi}{2F}] \\ V'_2 = -2V_p M \sec \frac{\pi}{2F} \sin \frac{(1-D-d)\pi}{2F} \sin \frac{(D+d)\pi}{2F} \end{cases} \quad (9)$$

By matching Equations (6) with (9), the values of  $x$  and  $y$  can be determined.

The principle of FTM-II for  $d < 0$  is illustrated in Figure 7. Similar to FTM-I for step-down of  $D$ , the actual transient process starts from Mode 2 rather than Mode 1. Based on the transient trajectory, Mode 2 ( $P_1 - P'_2$ ) is completed earlier so that Mode 3 can move into one side of  $(D + d)$ -loop. By ending Mode 3 right on the boundary point, a new steady-state period begins at  $P'_3$ .

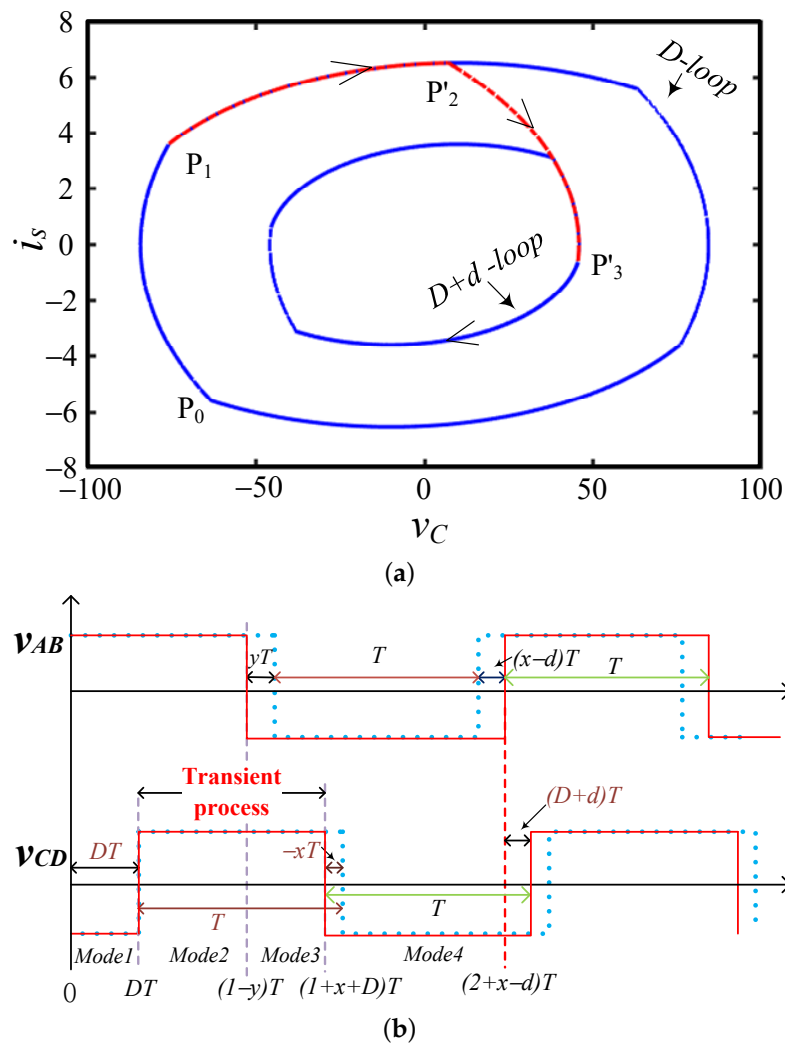


**Figure 7.** Principle of FTM-II with two steps for  $d < 0$ : (a) the transient trajectory of  $i_s$  and  $v_C$ ; (b) the transient waveforms of  $v_{AB}$  and  $v_{CD}$ .

In conclusion, FTM-II consists of two different modes. For the case of  $d > 0$ , both  $x$  and  $y$  are positive.  $v_{AB}$  is shifted to the left by  $yT$  by reducing its positive pulse once and two consecutive edges of  $v_{CD}$  are delayed by  $xT$  and  $(d - y)T$ . For the case of  $d < 0$ ,  $x$  is negative and  $y$  is still positive.  $v_{CD}$  is shifted to the left by  $-xT$  by reducing its positive pulse once and two consecutive edges of  $v_{AB}$  are shifted earlier by  $yT$  and delayed by  $(x - d)T$  respectively. If  $d > 0$ ,  $v_{AB}$  has two transient pulses, whose width is  $(1 - y)T$  and  $(1 + x - y - d)T$  respectively.  $v_{CD}$  only has one transient pulse with the width at  $(1 + x)T$ . If  $d < 0$ ,  $v_{CD}$  has two transient pulses, whose widths are  $(1 + x)T$  and  $(1 - x - y + d)T$  respectively.  $v_{AB}$  only has one transient pulse with the width at  $(1 - y)T$ . The durations of each mode in the transient process are concluded in Table 2.

**Table 2.** The durations of each mode using FTM-II.

	$d > 0$	$d < 0$
Mode 1	$(D + x)T$	$DT$
Mode 2	$(1 - D - x - y)T$	$(1 - D - y)T$
Mode 3	$(D + d)T$	$(D + x + y)T$
Mode 4	$(1 - D - d)T$	$(1 - D - d)T$

### 4. Simulation and Experimental Verification

To verify the feasibility of the proposed method, the step transient process of a DBSRC is simulated in PSIM. The specifications of the DBSRC in simulation and experiment are given in Table 3. The two phase-shift ratios are  $D_1 = 1/6$  and  $D_2 = 1/3$ .

**Table 3.** Specifications of the DBSRC.

Parameters	Symbol	Value
primary voltage	$V_p$	60 V
secondary voltage	$V_s$	50 V
switching frequency	$f_s$	100 kHz
resonant inductor	$L_r$	31.035 $\mu$ H
resonant capacitor	$C_r$	137.93 nF
transformer turns ratio	$n_t:1$	1:1

The simulation results for DTM, FTM-I, FTM-II are given in Figure 8. For each method, two cases of step-up and step-down of  $D$  are tested. For each case, the waveforms of  $v_{AB}, v_{CD}, i_s, v_C$  are recorded. On one side, waveforms of  $i_s$  and  $v_C$  using DTM show long-term oscillation with high overshoot current/voltage. On the other side, the two FTM methods give much better performance as the theoretical analysis predicts. Both step-up and step-down transient processes can be completed within one HF cycle. Moreover, there is no overshoot current/voltage shown in the process. In addition, the dynamic performance of DBSRC with a conventional PI controller and FTM are compared. The simulation results are shown in Figure 9, where two cases of a same step-up of  $D$  with a PI controller and FTM-I are illustrated. The waveforms from up to bottom are  $D, i_s$  and  $v_C$ , respectively. It can be found that FTM is advantageous over conventional PI control in terms of response speed or total transient duration, since FTM (step change of  $D$ ) only uses one HF period while the conventional PI controller has longer transient duration due to the small-step increasing of  $D$ .

In the lab, a prototype converter with same specifications as Table 3 is built for further verifications. A DC power supply EA-PS 9500-10 is used to generate  $V_p$  while  $V_s$  is obtained from a DC electronic load EA-EL 9750-60B in CV mode. The transient control scheme is implemented in a TMS320F28335 DSP board. In steady state, the measured resonant current  $i_s$  and resonant capacitor voltages  $v_C$  are 4.0 A and 54.5 V for  $D = 1/6$ , respectively. At  $D = 1/3$ , those two steady-state values become 6.65 A and 86.5 V, respectively.

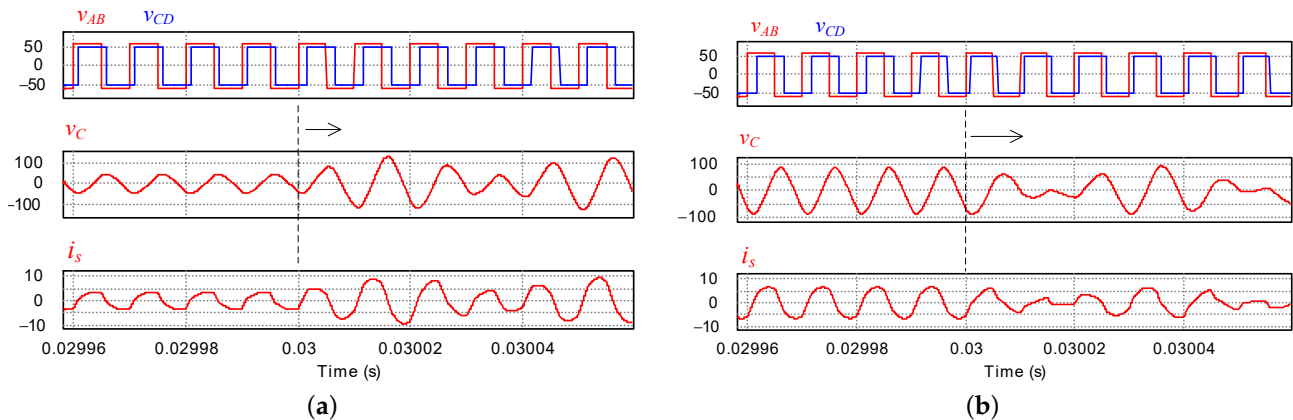


**Figure 8.** Cont.

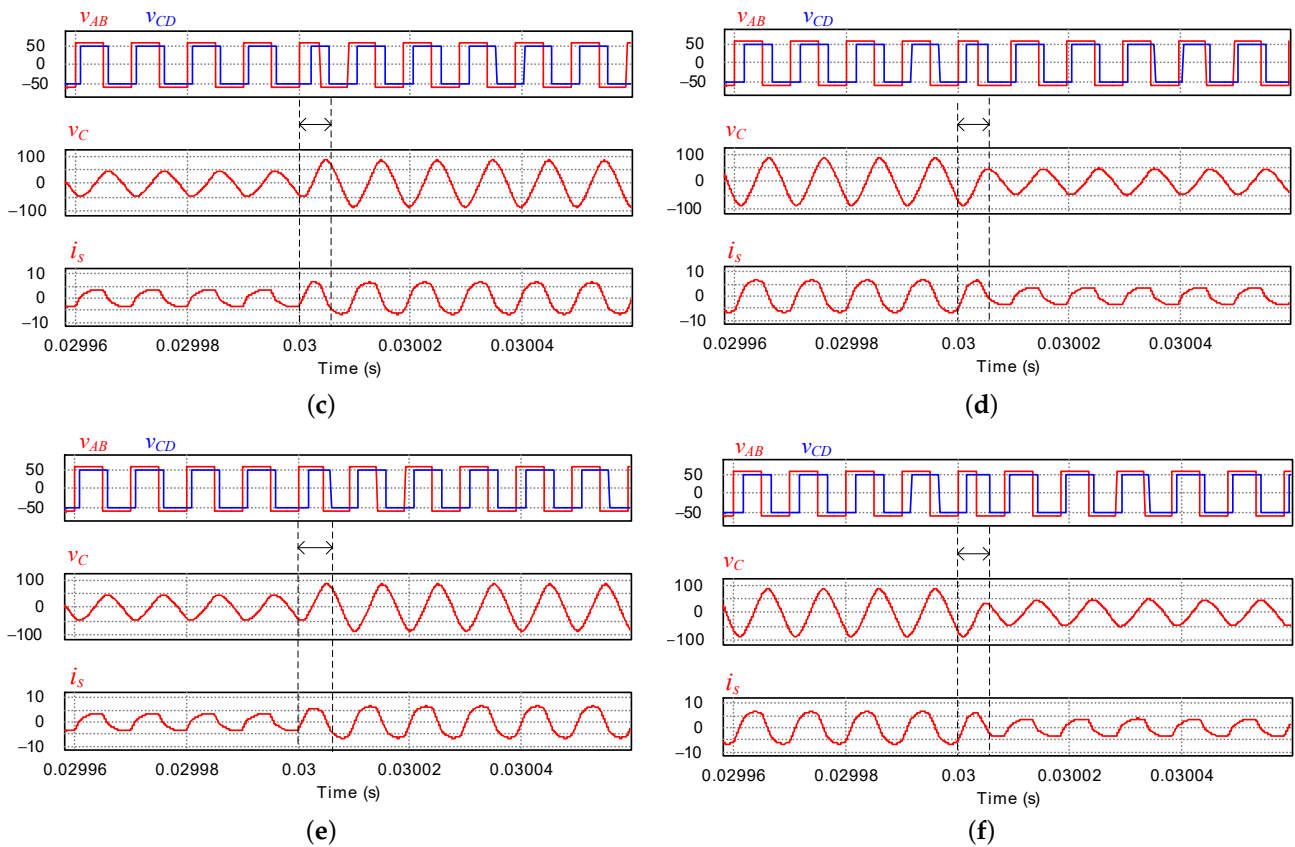


**Figure 8.** Simulated waveforms for (a) step-up of  $D$  with DTM, (b) step-down of  $D$  with DTM, (c) step-up of  $D$  with FTM-I, (d) step-down of  $D$  with FTM-I, (e) step-up of  $D$  with FTM-II, (f) step-down of  $D$  with FTM-II.

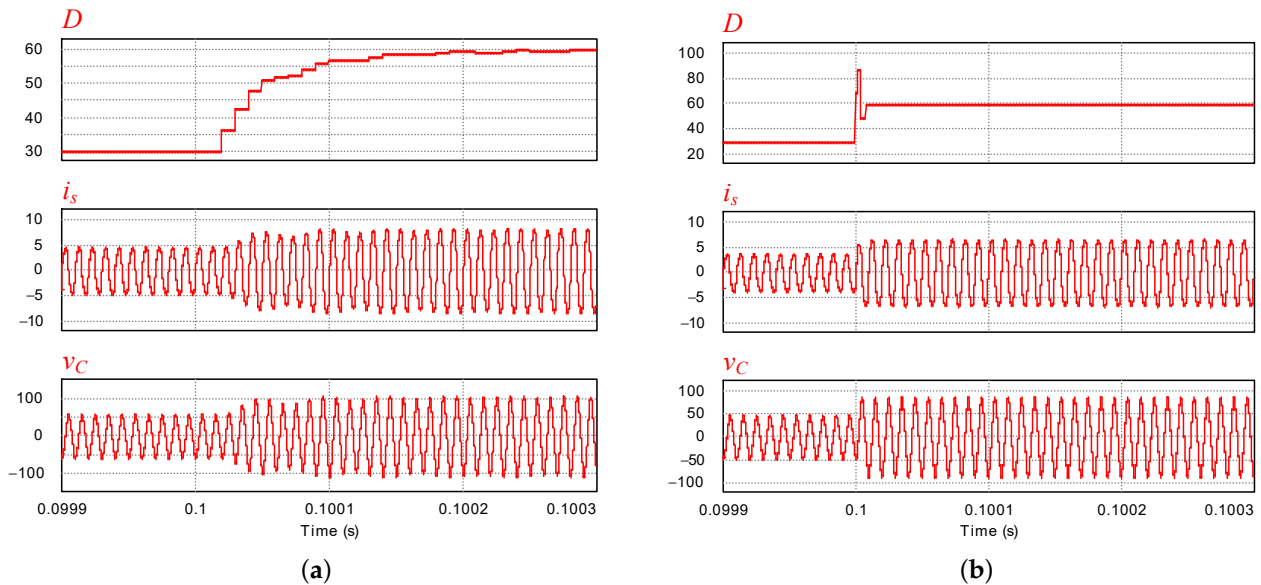


**Figure 9.** Simulated waveforms for (a) PI controller, (b) FTM-I.

First, the two-step changes of  $D$  using DTM are evaluated, and the transient waveforms are captured. For step-up of  $D$  in Figure 10a, an overshoot voltage and current of 21.5 V and 1.4 A are identified and the oscillation in the transient process lasts for almost 11 HF cycles. The similar phenomena of oscillation can be viewed in the case of the step-down of  $D$  shown

in Figure 10b. The illustrated corresponding  $i_s - v_C$  trajectories confirm that the DTM is not a good selection due to long transient duration, and high overshoot voltage/current.

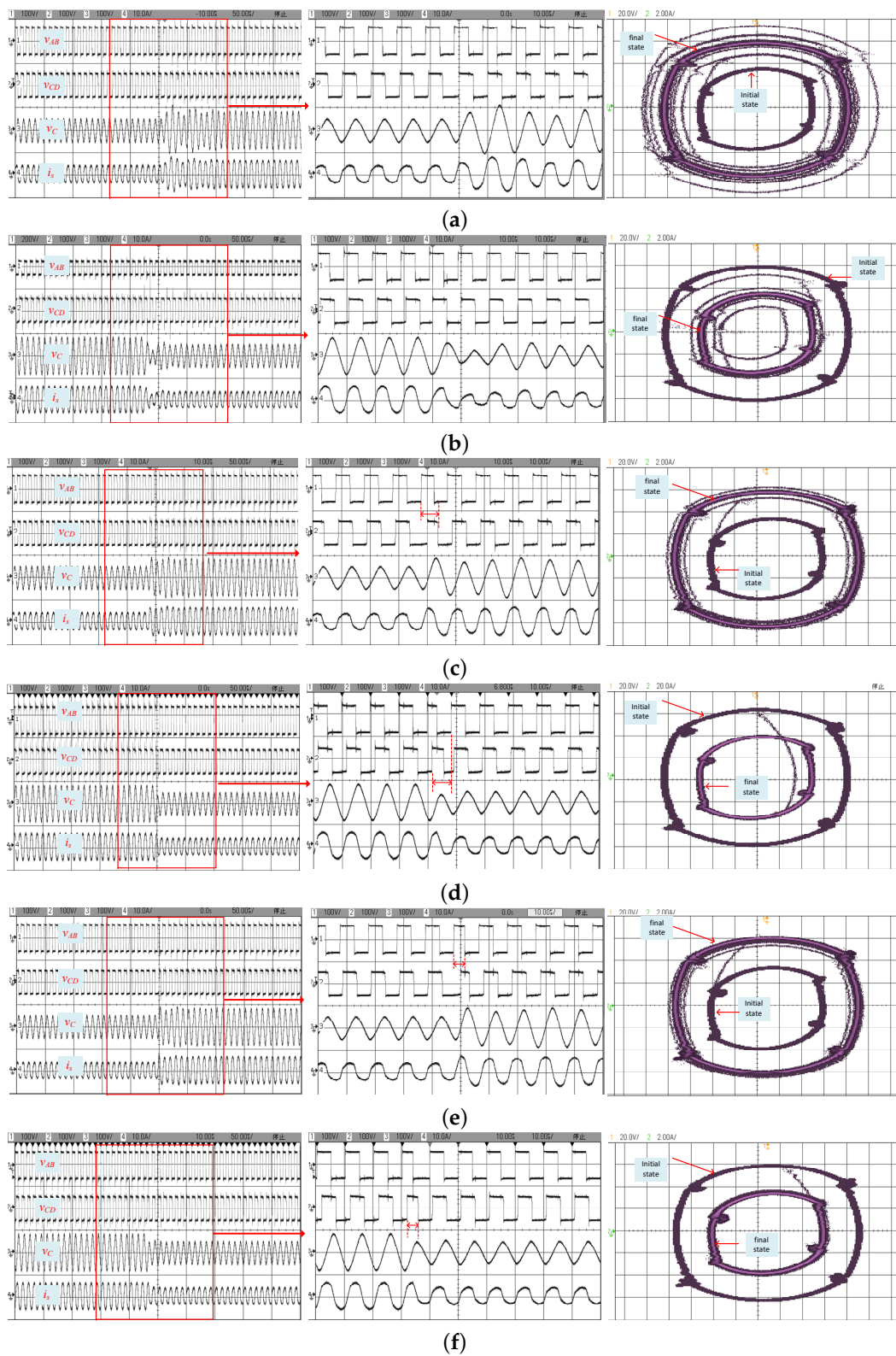


**Figure 10.** Experimental waveforms for (a) step-up of  $D$  with DTM, (b) step-down of  $D$  with DTM, (c) step-up of  $D$  with FTM-I, (d) step-down of  $D$  with FTM-I, (e) step-up of  $D$  with FTM-II, (f) step-down of  $D$  with FTM-II.

The experimental plots for the step-up of  $D$  using FTM-I are presented in Figure 10c. The values of  $x$  and  $y$  are found to be 0.777 and 0.444, respectively. A fast transient response can be achieved, which is apparently much improved compared with DTM. Due to the non-ideality of actual circuit, the transient process also lasted for more than one switching cycle, which can be identified easily from the trajectory. There is also small overshoot voltage/current. The case for the step-down of  $D$  using FTM-I is presented in Figure 10d. The values of  $x$  and  $y$  are found as 0.777 and 0.444, respectively. The obtained trajectory is almost the same as the theoretical one. The whole transient process is completed in three modes as marked in the plot and no oscillation can be viewed.

In Figure 10e,f, the two-step-change cases using FTM-II are illustrated. As with FTM-I, the performance of the step-up case shows some deviations, where there are some oscillations after the transient modulation is done. On the other side, the step-down of  $D$  can be accomplished without noticeable error.

The comparison of the experimental results of the three methods is concluded in Table 4. The overshoot current and overshoot voltage are given in terms of both actual value and percentage. The overshoot values for step-down case are calculated using the final steady-state values as the reference. The performance of two FTM-based methods is pretty close, while the conditions of step-down cases look better than that of the step-up cases with almost negligible oscillation. Because many non-ideal factors are involved in the experimental test, there is a gap between the experimental results and the idealized simulation results. The deviation of resonant component values can be a main potential reason, which affects the accurate calculation of  $x$  and  $y$ . Moreover, the actual dead-band in gating signals can bring some errors too if the values of  $x$  and  $y$  are quite small. However, the experimental results still show the superiority of the proposed FTM-based methods. First, compared with DTM, the proposed FTM-I and FTM-II have significantly lower overshoot current and voltage. The overshoot current/voltage is restrained to a certain extent. Second, the proposed FTM-I and FTM-II are faster than DTM, which also shows that FTM-I and II have better transient performance.

**Table 4.** The experimental comparison of the three methods.

Method	DTM	FTM-I	FTM-II
Step-up of $D$ from 1/6 to 1/3:			
$x$	n/a	0.2154	0.2799
$y$	n/a	0.1002	0.2375
overshoot current	1.4 A (21.5%)	0.15 A (2.26%)	0.1 A (1.5%)
overshoot voltage	21.5 V (24.86%)	3.5 V (4.05%)	2.5 V (2.89%)
transient duration	11	6	4
Step-down of $D$ from 1/3 to 1/6:			
$x$	n/a	−0.1737	−0.2411
$y$	n/a	0.3208	0.2487
overshoot current	0.5 A (12.5%)	0.13 A (3.25%)	0.10 A (2.5%)
overshoot voltage	8.50 V (15.6%)	0.70 V (1.288%)	0.50 V (0.92%)
transient duration	6	4	2

## 5. Conclusions

For a DBSRC, transient oscillations may depress dynamic performance and output voltage quality. Furthermore, the DC bias current caused by the oscillations may increase the current stress of transformers and affect the reliability of converters. Thus, this paper proposes two methods based on fast transient modulation (FTM) to address these concerns. The operating principle and steady-state trajectory of DBSRC with phase-shift control were

analyzed first. Then, two FTM methods were comprehensively presented. In terms of resonant voltage-current trajectory, the transient route of FTM is identified and limited between two steady-state loops. Therefore, one of the advantages of the methods is no overshoot current or voltage existing in the transient process. Since FTM enables the converter to enter the new steady state within one switching cycle theoretically, another advantage of the methods is that the converter has a high-quality and ultrafast dynamic response. Moreover, the detailed discussion and clear explanation about how to modulate the phase-shift ratio for the step-load-change transient under two FTM methods are provided, which can be regarded as guidance for industrial design and operation.

Compared with the conventional direct transient modulation, as demonstrated by both simulations and experiments, the proposed two FTM methods show obvious superiority in terms of the overshoot current/voltage and transient duration. The trade-off is that the determination of  $x$  and  $y$  is complicated and currently they can be pre-calculated and stored as a look-up table. More efforts will be made to simplify the calculation or find an alternative way to determine the suitable transient adjustment of gating signals.

**Author Contributions:** Conceptualization, H.X.; Data curation, S.Z.; Formal analysis, H.X.; Funding acquisition, S.H.; Investigation, H.C.; Methodology, H.X.; Project administration, X.L.; Software, S.Z.; Supervision, X.L.; Validation, S.H.; Visualization, H.C.; Writing—original draft, H.X.; Writing—review and editing, S.H. All authors have read and agreed to the published version of the manuscript.

**Funding:** This research was funded in part by National Natural Science Foundation of China under Grant No. 62003057, in part by FDCT under Grant No. 0065/2019/A2, in part by Natural Science Foundation of Jiangsu Province under Grant No. BK20191029, and in part by the Natural Science Foundation of Jiangsu Higher Education Institutions of China under Grant No. 19KJB470001.

**Conflicts of Interest:** The authors declare no conflict of interest.

## References

1. Hazari, M.R.; Jahan, E.; Mannan, M.A.; Das, N. Transient Stability Enhancement of a Grid-Connected Large-Scale PV System Using Fuzzy Logic Controller. *Electronics* **2021**, *10*, 2437. [[CrossRef](#)]
2. Ramadan, A.; Ebeed, M.; Kamel, S.; Mosaad, M.I. Abu-Siada, A. Technoeconomic and Environmental Study of Multi-Objective Integration of PV/Wind-Based DGs Considering Uncertainty of System. *Electronics* **2021**, *10*, 3035. [[CrossRef](#)]
3. Inoue, S.; Akagi, H. A Bidirectional Isolated DC-DC Converter as a Core Circuit of the Next-Generation Medium-Voltage Power Conversion System. *IEEE Trans. Power Electron.* **2007**, *22*, 535–542. [[CrossRef](#)]
4. Zhao, B.; Song, Q.; Liu, W. Overview of Dual-Active-Bridge Isolated Bidirectional DC-DC Converter for High-Frequency-Link Power-Conversion System. *IEEE Trans. Power Electron.* **2014**, *29*, 4091–4106. [[CrossRef](#)]
5. Wu, J.; Li, X.; Zhou, S.; Hu, S.; Chen, H. Constant-current, constant-voltage operation of a dual-bridge resonant converter: Modulation, design and experimental results. *Appl. Sci.* **2021**, *11*, 12143. [[CrossRef](#)]
6. Li, X.; Bhat, A. Analysis and Design of High-Frequency Isolated Dual-Bridge Series Resonant DC/DC Converter. *IEEE Trans. Power Electron.* **2014**, *25*, 850–862.
7. Agamy, M.; Dong, D.; Garces, L.; Zhang, Y.; Dame, M.; Wu, X.; Pan, Y. A High Power Medium Voltage Resonant Dual Active Bridge for MVDC Ship Power Networks. *IEEE J. Emerg. Sel. Top. Power Electron.* **2017**, *5*, 88–99. [[CrossRef](#)]
8. Wang, S.; Zheng, Z.; Li, C.; Xu, L.; Wang, K.; Li, Y. Accurate Frequency-domain Analysis and Hybrid Control Method for Isolated Dual Active Bridge Series Resonant DC/DC Converters. *IEEE Trans. Power Electron.* **2019**, *12*, 2932–2941. [[CrossRef](#)]
9. Chen, G.; Li, X.; Zhou, S. Unified Boundary Control With Phase Shift Compensation for Dual Bridge Series Resonant DC-DC Converter. *IEEE Access* **2020**, *8*, 131137–131149. [[CrossRef](#)]
10. Shao, S.; Chen, H.; Wu, X.; Zhang, J.; Sheng, K. Circulating Current and ZVS-on of a Dual Active Bridge DC-DC Converter: A Review. *IEEE Access* **2019**, *7*, 50561–50572. [[CrossRef](#)]
11. Yaqoob, M.; Loo, K.H.; Lai, Y.M. A Four-Degree-Of-Freedom Modulation Strategy for Dual-Active-Bridge Series-Resonant Converter Designed for Total Loss Minimization. *IEEE Trans. Power Electron.* **2019**, *34*, 1065–1081. [[CrossRef](#)]
12. Duy-Dinh, N.; Tuyen, N.D.; Goto, F.; Toshihisa, F. Dual-active-bridge Series Resonant Converter: A New Control Strategy Using Phase-shifting Combined Frequency Modulation. In Proceedings of the 2015 IEEE Energy Conversion Congress and Exposition, Montreal, QC, Canada, 20–24 September 2015; pp. 1215–1222.
13. Shi, H.; Wen, H.; Hu, Y.; Jiang, L. Reactive Power Minimization in Bidirectional DC-DC Converters using a Unified-phasor-based Particle Swarm Optimization. *IEEE Trans. Power Electron.* **2018**, *33*, 10990–11006. [[CrossRef](#)]
14. Hu, S.; Li, X.; Bhat, A.K.S. Operation of a Bidirectional Series-Resonant Converter with Minimized Tank Current and Wide ZVS Range. *IEEE Trans. Power Electron.* **2019**, *34*, 904–915. [[CrossRef](#)]

15. Hu, S.; Li, X.; Zheng, Q.-F. A Dual-Bridge DC-DC Resonant Converter Using Extended PWM and Phase-Shift Control. *IEEE Trans. Ind. Appl.* **2021**, *57*, 4009–4020. [[CrossRef](#)]
16. Mirzahosseini, R.; Tahami, F. Phase-shift Three-phase Bidirectional Series Resonant DC/DC Converter. In Proceedings of the 2011 37th Anniversary Conference of IEEE Industrial Electronics, Melbourne, Australia, 7–10 November 2011; pp. 1137–1143.
17. Seltzer, D.; Corradini, L.; Bloomquist, D.; Zane, R.; Maksimovi, D. Small Signal Phasor Modeling of Dual Active Bridge Series Resonant DC/DC Converters with Multi-angle Phase-shift Modulation. In Proceedings of the 2011 IEEE Energy Conversion Congress and Exposition, Phoenix, AZ, USA, 17–22 September 2011; pp. 2757–2764.
18. Song, W.; Zhong, M.; Luo, S.; Yang, S. Model Predictive Power Control for Bidirectional Series-Resonant Isolated DC-DC Converters with Fast Dynamic Response in Locomotive Traction System. *IEEE Trans. Transp. Electr.* **2020**, *6*, 1326–1337. [[CrossRef](#)]
19. Engel, S.P.; Soltan, N.; Stagge, H.; De Doncker, R.W. Dynamic and balanced control of three-phase high-power dual active bridge dc-dc converters in dc-grid applications. *IEEE Trans. Power Electron.* **2013**, *28*, 1880–1889. [[CrossRef](#)]
20. Bu, Q.; Wen, H.; Shi, H.; Zhu, Y. A Comparative Review of High-Frequency Transient DC Bias Current Mitigation Strategies in Dual-Active-Bridge DC-DC Converters Under Phase-Shift Modulations. *IEEE Trans. Ind. Appl.* **2021**. [[CrossRef](#)]
21. Li, X.; Li, Y.F. An Optimized Phase-shift Modulation for Fast Transient Response in a Dual-active-bridge Converter. *IEEE Trans. Power Electron.* **2014**, *29*, 2661–2665. [[CrossRef](#)]
22. Tang, Y.; Li, X.; Zhou, S.; Sun, C.; Chen, G. Comprehensive Study of Fast Load Modulation with Volt-second Balance in a Dual-active-bridge Converter. *IET Power Electron.* **2019**, *12*, 1357–1367. [[CrossRef](#)]
23. Zhao, B.; Song, Q.; Liu, W.; Zhao, Y. Transient DC Bias and Current Impact Effects of High-Frequency-Isolated Bidirectional DC-DC Converter in Practice. *IEEE Trans. Power Electron.* **2016**, *31*, 3203–3216. [[CrossRef](#)]
24. Bu, Q.; Wen, H.; Wen, J.; Hu, Y.; Du, Y. Transient DC Bias Elimination of Dual-Active-Bridge DC-DC Converter With Improved Triple-Phase-Shift Control. *IEEE Trans. Ind. Electron.* **2020**, *67*, 8587–8598. [[CrossRef](#)]
25. Yang, C.; Wang, J.; Wang, C.; You, X.; Xu, L. Transient DC Bias Current Reducing for Bidirectional Dual-Active-Bridge DC-DC Converter by Modifying Modulation. *IEEE Trans. Power Electron.* **2021**, *36*, 13149–13161. [[CrossRef](#)]
26. Wang, S.; Li, C.; Wang, K.; Zheng, Z.; Li, Y. Loss Imbalance and Transient DC-Bias Mitigation in Dual-Active-Bridge DC/DC Converters. *IEEE J. Emerg. Sel. Top. Power Electron.* **2021**, *9*, 1399–1409. [[CrossRef](#)]
27. Ma, S.; Guo, Z.; Luo, Y. Universal Modulation Scheme to Suppress Transient DC Bias Current in Dual Active Bridge Converters. *IEEE Trans. Power Electron.* **2022**, *37*, 1322–1333.
28. Sun, C.; Jiang, X.; Cao, L.; Loo, K.H. Total Suppression of High-Frequency Transient Oscillations in Dual-Active-Bridge Series-Resonant Converter by Trajectory-Switching Modulation. *IEEE Trans. Power Electron.* **2022**, *37*, 6511–6529. [[CrossRef](#)]
29. Fei, C.; Lee, F.C.; Li, Q. Digital Implementation of Soft Start-Up and Short-Circuit Protection for High-Frequency LLC Converters With Optimal Trajectory Control. *IEEE Trans. Power Electron.* **2017**, *32*, 8008–8017. [[CrossRef](#)]
30. Duan, R.; Yuan, L.; Gu, Q.; Nie, J.; Zhao, Z. Trajectory-Prediction-Based Fast Bidirectional Power Transient Control for Series Resonant Dual-Active-Bridge Converter. In Proceedings of the IEEE Energy Conversion Conference and Exposition, Portland, OR, USA, 23–27 September 2018; pp. 1415–1422.
31. Xu, H.; Zhou, S.-Z.; Li, X.; Chen, H.; Hu, S. Fast Transient Modulation of a Dual-Bridge Series Resonant Converter. In Proceedings of the IECON 2021—47th Annual Conference of the IEEE Industrial Electronics Society, Toronto, ON, Canada, 13–16 October 2021; pp. 1–6.